10-10-2012

Spectroscopic and Computational Studies of Matrix-Isolated iso-CXBr3 (X=F,Cl,Br): Structure, Properties, and Photochemistry of Substituted Iso-Tribromomethanes

Lisa George
Marquette University

Aimable Kalume
Marquette University, aimable.kalume@marquette.edu

Scott Reid
Marquette University, scott.reid@marquette.edu

Brian J. Esselman
University of Wisconsin-Madison

Robert J. McMahon
University of Wisconsin-Madison

Accepted version. *Journal of Molecular Structure,* Vol. 1025, (October 2012): 61–68. DOI:

Spectroscopic and Computational Studies of Matrix-isolated Iso-$CXBr_3$ (X = F, Cl, Br): Structure, Properties, and Photochemistry of Substituted Iso-tribromomethanes

Lisa George
Department of Chemistry, Marquette University, Milwaukee, WI
Aimable Kalume
Department of Chemistry, Marquette University, Milwaukee, WI
Scott A. Reid
Department of Chemistry, Marquette University, Milwaukee, WI
Brian J. Esselman
Department of Chemistry, University of Wisconsin-Madison, Madison, WI
Robert J. McMahon
Department of Chemistry, University of Wisconsin-Madison, Madison, WI

Abstract

Iso-polyhalomethanes are important reactive intermediates in the condensed and gas-phase chemistry of halomethanes. Building upon our recent study of iso-bromoform, in this work the substituted iso-

tribromomethanes (iso-$CXBr_3$; X = F, Cl, Br) were characterized by matrix isolation infrared and UV/Vis spectroscopy, supported by *ab initio* calculations, to further probe the structure, spectroscopy, properties, and photochemistry of these important intermediates. Selected wavelength laser irradiation of $CXBr_3$ samples in an inert rare gas (typically Ar; mixing ratio 1:500) held at ~5 K yielded iso-$CXBr_3$ (XBrC–Br–Br or Br_2C–Br–X). The observed infrared and UV/Vis absorptions are in excellent agreement with computational predictions, and the energies of various stationary points on the $CXBr_3$Potential Energy Surfaces (PESs) were characterized computationally using DFT, MP2, and CCSD (T) methods in combination with triple-zeta quality basis sets. These calculations show that the isomers are minima on the PESs that lie ~200 kJ/mol above the global $CXBr_3$ minimum, yet are bound by some 50–70 kJ/mol in the gas-phase with respect to the $CXBr_2$ + Br asymptote. Laser irradiation of the isomers resulted in back photoisomerization to $CXBr_3$, and intrinsic reaction coordinate (IRC) calculations confirmed the existence of a first order saddle point connecting the two isomers. Calculations of important stationary points on the $CXBr_3$ PESs show that in the gas-phase the isomerization barrier lies energetically near the threshold for simple bond fission. The iso-$CXBr_3$species are significantly stabilized in the condensed phase, due to the high degree of ion-pair character, as revealed by Natural Resonance Theory analysis.

Keywords

Iso-polyhalomethanes, Photoisomerization, Matrix isolation, Ion-pair

1. Introduction

Reflecting their widespread industrial use and ozone-depleting potential, the photochemistry of bromine-containing halocarbons (halons) has been intensely studied in both gas and condensed phases.[1], [2], [3], [4], [5], [6], [7], [8], [9], [10], [11], [12], [13], [14], [15], [16], [17], [18] Bromoform ($CHBr_3$) and its derivatives are among the most important of these halons; indeed, bromoform is a primary producer of bromine in the troposphere and mid-latitude lower stratosphere.[6], [7], [8], [12] In condensed phases, the photolysis of bromoform is known to lead to facile production of iso-bromoform (HBrCBr–Br) following geminate recombination of the initially formed radical pair in the solvent cage. To our knowledge, the first observation of the iso-species occurred in UV irradiated glasses containing halomethanes, which exhibited “color centres” that were assigned first to trapped electrons, [19] and later to trapped ions.[20] The isomer of bromoform plays a pivotal role in the solution phase photochemistry;[14], [15] for example, Phillips and co-workers showed using picosecond time-resolved Resonance Raman (TR3) spectroscopy that in aqueous solution the isomer reacts with water to yield a $CHBr_2OH$ reaction product and a HBr leaving group.[14] Subsequently, the same authors showed that the photolysis of bromoform in water led to essentially complete conversion to HBr, and involved the water-catalyzed O–H insertion/HBr elimination reaction of isobromoform.[15] Recently, ultrafast transient absorption studies of the formation and decay of iso-bromoform in solution have been reported.[18]

In a recent study, we examined the spectroscopy, structure, and properties of iso-bromoform using matrix isolation techniques, supported by high level calculations [21] Laser irradiation of bromoform isolated in Ar or Ne matrices at ~5 K yielded iso-$CHBr_3$; the observed infrared and UV–Vis absorptions were in excellent agreement with computational predictions. Gas-phase calculations showed that the isomer well lies 200 kJ/mol above the global $CHBr_3$ minimum, and 60 kJ/mol below the $CHBr_2$ + Br asymptote. The photochemistry of iso-$CHBr_3$ was investigated by laser irradiation into the intense $S_0 \rightarrow S_3$ transition, which resulted in back isomerization to $CHBr_3$. Intrinsic reaction coordinate (IRC) calculations confirmed the existence of a first order saddle point connecting the two isomers; the predicted isomerization barrier lies below the energetic threshold of the radical channel.[22] Natural Bond Orbital (NBO) analysis and Natural Resonance Theory (NRT) were used to characterize the important resonance structures of the isomer and related stationary points. These calculations show that the isomerization transition state represents a cross-over from dominantly covalent to dominantly ionic (ion-pair) bonding.

In comparison with bromoform, less is known about the substituted tribromomethanes iso-$CXBr_3$(X = F, Cl, Br, I). Following the pioneering work of Maier and co-workers,[23], [24], [25] Phillips and co-workers studied the vibrational spectra of iso-$CXBr_3$ (X = F, Br) in solution using picosecond TR3 spectroscopy, supported by DFT,[26]

which characterized several fundamental vibrational frequencies for each species. Later, the same group examined the photolysis of CBr_4 in water and acetonitrile/water solution, and showed that the water catalyzed O–H insertion/H–Br elimination reaction of iso-CBr_4 led to the final products: HBr and CO_2.[27] The TR3 experiments revealed that, following UV photolysis, iso-CBr_4 is formed on the ps timescale, and persists for several ns in acetonitrile/water solution.

Rentzepis and co-workers examined the photochemistry of CBr_4 in various solvents using ultrafast time-resolved spectroscopy.[28] Following 266 or 267 nm excitation, a broad absorption feature near 480 nm appeared promptly and persisted for hundreds of ns in cyclohexane solution. Based upon the shift in the absorption maximum with solvent dielectric constant, the carrier of this band was assigned to a cation, in particular a solvent stabilized (and solvent separated) CBr3++Br- ion pair. It was conjectured that the solvent separation prevented fast recombination of the ions, leading to the observed stability. Despite earlier work on the iso-polyhalomethanes, the assignment of the 480 nm feature to iso-CBr_4 was not considered. Later, Ihee and co-workers examined the photolysis of CBr_4 in methanol using time-resolved X-ray diffraction,[29] and reported no evidence for isomer formation within the signal to noise of their experiment. In this case the dominant species observed 100 ps after photolysis was CBr_3 + Br, and it was suggested that these radicals recombined in a non-geminate reaction to form C_2Br_6 and Br_2. In a purely theoretical paper, the same group calculated vibrational frequencies and electronic absorptions of iso-CBr_4 and other potential CBr_4 photolysis products using DFT methods.[30]

In this study, we report matrix isolation studies of the iso-$CXBr_3$ (X = F, Cl, Br) species, and have characterized the electronic spectroscopy of these systems for the first time. We report both infrared and UV–Vis spectra of the isomers, which were generated in good yield following laser irradiation of the parent compounds trapped in rare gas matrices at low temperature. The photochemistry of the isomers was investigated by selected wavelength laser irradiation. Our experimental results are supported by extensive ab initio calculations using density functional and post-Hartree Fock methods, which shed significant light on the structure and properties of the isomers.

2. Experimental and theoretical methods

The matrix isolation experiments utilized an apparatus that has been described in detail in recent articles,[21], [31] and therefore only details pertinent to this study will be reported. Samples of $CXBr_3$(X = F, Cl, Br) in a rare gas (typically Ar) at typical mixing ratios of 1:500 were prepared by passing the high purity rare gas at a typical pressure of 2 bar over the chemical held in a stainless steel bubbler (for $CFBr_3$) or a homemade solid sample holder (for $CClBr_3$ and CBr_4). The $CFBr_3$ sample (Alpha Aesar, 99%) was placed in a refrigerated bath held at 254 K. $CClBr_3$ was prepared as described below, while CBr_4 was used as supplied (TCI America, 99%). The gas mixtures were deposited onto the cold window held at ~5 K using the pulsed deposition method with a solenoid actuated pulsed valve; typical conditions were: 1 ms pulse duration, 5 Hz repetition rate, 1 h deposition time, 2 bar backing pressure. Before each experiment the sample line was pumped under vacuum in order to remove volatile impurities.

Following deposition, the cold window was irradiated with laser light at 230 nm (for $CFBr_3$) and 220 nm (for $CClBr_3$ and CBr_4), generated from the frequency doubled output of a dye laser system (Lambda-Physik Scanmate 2E) operating on Coumarin 460 or 440 dye, pumped by the third harmonic (355 nm) of a Nd:YAG laser (Continuum NY-61). In some of the $CFBr_3$ experiments the 266 nm output of a second Nd:YAG laser (Continuum Minilite) was used as the photolysis source. In either case, the photolysis beam was expanded using a 4:1 beam expander to fill the cold window and avoid damage to the outer KBr windows. Typical irradiation times were on the order of 1 h. Infrared (IR) absorption spectra were recorded with a Mattson Galaxy series FTIR at typically 2 cm^{-1} resolution and averaged over 128 scans. Ultraviolet/Visible (UV–Vis) absorption spectra were obtained with an Agilent 8453 diode array spectrophotometer. The reference spectra for both IR and UV–Vis were recorded for the cold sample holder immediately prior to matrix deposition, and the cryostat was mounted on a home-built rail system that allowed quick interchange between spectrometers. All spectra were transferred to a spreadsheet and analysis program (Origin 8.0) for subsequent workup.

The $CClBr_3$ sample was prepared according to the following procedure.[32] To a round-bottom flask equipped with a magnetic stir-bar and a rubber septum were added $CHBr_3$ (10.1 g, 40 mmol) and 4–6% aqueous sodium hypochlorite (200 mL). The resulting mixture was stirred vigorously for 3 days at 22 °C and the granular solid thus formed was filtered and washed repeatedly with water (4 × 100 mL) to afford 5.8 g (70%) of white solid; ^{13}C NMR (400 MHz, $CDCl_3$) δ:3.8.

Calculations were typically carried out using the Gaussian 09 electronic structure package on the MU Pere cluster.[33] In addition, some calculations were performed using the GAMESS electronic structure package on the COBALT (SGI Altix) system at the National Center for Supercomputing Applications. Geometry optimization was typically performed using the B3LYP, M06, and MP2 methods with an aug-cc-pVXZ basis set; harmonic vibrational frequencies and infrared intensities were calculated at the same levels of theory. All frequencies reported in this work are unscaled. Subsequently, single point energy calculations were performed at the CCSD(T)/aug-cc-pVTZ level of theory using the optimized MP2/aug-cc-pVTZ structures. NBO calculations were carried out on the Department of Chemistry (Phoenix) Cluster at UW-Madison using Gaussian 09 with NBO version 5.9.[34]

3. Results and discussion

3.1. Infrared and UV–Vis spectroscopy of iso-$CXBr_3$

Fig. 1 shows matrix IR (upper panel) and UV–Vis spectra of a $CFBr_3$:Ar (~1:500) sample at 5 K following laser photolysis at 230 nm and annealing to 33 K. Also shown in each panel as stick spectra are Density Functional Theory (DFT) and Time-Dependent DFT (TDDFT) predictions of the spectra of iso-$CFBr_3$(FBrC–Br–Br). This compound is the dominant species produced upon photolysis in the matrix, and the positions and relative intensities of the observed IR absorptions are in excellent agreement with theoretical predictions and with previous results from time-resolved Resonance Raman spectroscopy (Table 1).[26] Note that the calculated vibrational frequencies using DFT methods (B3LYP, M06) with an aug-cc-pVTZ basis set are in nearly quantitative agreement with experiment (Table 1), whereas the MP2 frequencies are overestimated by up to ~10%. The important equilibrium structural parameters for iso-$CFBr_3$ as derived from calculations (B3LYP/aug-cc-pVTZ) are shown in Fig. 2.

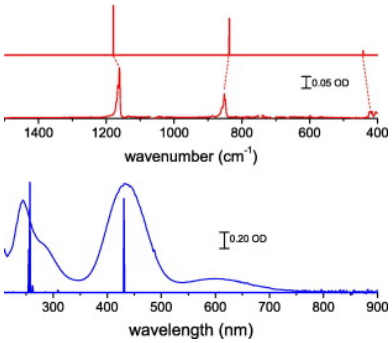

Fig. 1. Upper panel: Observed and calculated (M06/aug-cc-pVTZ) infrared spectrum of iso-$CFBr_3$ in an Ar matrix at 5 K (the bar denotes an absorbance of 0.05). Lower panel: Observed and calculated (TDM06/aug-cc-pVTZ) electronic spectrum of the isomer (bar denotes an absorbance of 0.20). The calculated spectra are in both panels shown as stick spectra and the intensities are arbitrarily scaled; quantitative information is provided in Table 1, Table 2.

Table 1. Observed and calculated (unscaled) vibrational frequencies (in cm^{-1}) of iso-$CFBr_3$. Calculations were performed with the methods shown and an aug-cc-pVTZ basis. Calculated intensities in km/mol are given in parentheses.

Mode	Approx. Descr.	Calc. (B3LYP)	Calc. (M06)	Calc. (MP2)	Obs. (this work; Ar [Ne])	Observed[26]
ν_1	C–F stretch	1179 (359)	1245 (410)	1201 (215)	1161 [1166]	–

ν_2	Asym. C–Br stretch	837 (265)	857 (245)	960 (157)	852 [856]	855
ν_3	C–F wag	442 (33)	439 (17)	467 (65)	421 [420]	419
ν_4	Sym. C–Br stretch	388 (44)	396 (52)	410 (21)	–	362
ν_5	F–C–Br bend	311 (14)	315 (16)	335 (4)	–	323
ν_6	Br–C–Br bend	189 (29)	190 (21)	231 (4)	–	204
ν_7	Br–Br stretch	164 (29)	161 (51)	198 (1)	–	171
ν_8	Torsion	79 (1)	82 (1)	86 (1)	–	–
ν_9	C–Br–Br bend	40 (4)	41 (5)	45 (1)	–	–

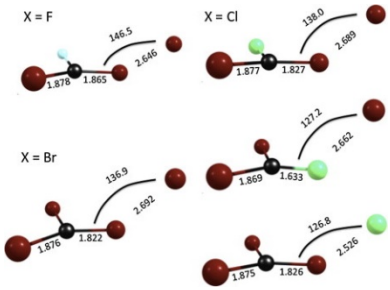

Fig. 2. Calculated structures of the iso-$CXBr_3$ (X = F, Cl, Br) species at the B3LYP/aug-cc-pVTZ level. Selected geometrical parameters are given. Bond angles are in degrees and bond lengths in Angstroms.

Table 2 provides a list of predicted vertical excitation energies and oscillator strengths of the lowest excited singlet states of iso-$CFBr_3$. Similar to other iso-polyhalomethanes, we find weak bands ($S_0 \rightarrow S_1$, S_2) in the visible region and a much stronger band ($S_0 \rightarrow S_3$) at higher energy. Under the assumption that the IR and UV–Vis spectra sample the same region of the matrix, the integrated IR and UV–Vis intensities were combined with calculated IR intensities to estimate the oscillator strength of the UV–Vis transitions. Thus, the integrated IR absorbance of a given feature was divided by the calculated intensity (in km/mol) to derive a column density in the matrix, and an average value was obtained over the observed IR absorptions. The oscillator strength of a given electronic (UV–Vis) band was then obtained according to the following formula.[21]

$$(1)\ f = (1.87 \times 10^{-7}\text{mol/km}) \times \frac{\int A_{elec}(\nu)d\nu}{N_{IR}}$$

where N_{IR} is the column density derived from the IR measurements and the numerator represents the integrated absorbance of a given electronic band. Using this approach, the derived oscillator strength of the most prominent band at 432 nm is 0.23 ($\varepsilon_{max} \sim$ 12,700 L mol^{-1} cm^{-1}), which is similar to the TD-CAM-B3LYP (f_{calc} = 0.27) and TD-M06 (f_{calc} = 0.23) predictions for the $S_0 \rightarrow S_3$ transition (Table 2). As found for other iso-polyhalomethanes, the TDDFT calculations tend to underpredict the intensity of the lowest energy ($S_0 \rightarrow S_1$, S_2) transitions.[21, 31] This may reflect intensity borrowing with the very strong $S_0 \rightarrow S_3$ transition.

Table 2. Observed and calculated electronic absorptions (in nm) of iso-$CXBr_3$. Calculations were performed using TDDFT with the noted functionals and an aug-cc-pVTZ basis set, using the B3LYP/aug-cc-pVTZ optimized geometries. Oscillator strengths are given in parentheses.

Species	**Assignment**	**Calc. (M06)**	**Calc. (CAM-B3LYP)**	**Obs. (this work; Ar)**
FBrC–Br–Br	S_1	657 (0.0001)	561 (0.0002)	594 (0.03)
	S_2	606 (0.0010)	521 (0.0006)	–
	S_3	431 (0.2325)	420 (0.2736)	432 (0.23)
	S_4	309 (0.0060)	295 (0.0002)	–
	S_5	286 (0.0023)	282 (0.1638)	288 (0.082)

	S_6	262 (0.0167)	252 (0.0016)	–
	S_7	257 (0.2727)	248 (0.0026)	–
	S_8	255 (0.1067)	243 (0.0746)	–
	S_9	226 (0.0018)	229 (0.2961)	–
	S_{10}	218 (0.0013)	201 (0.0182)	–
$Br_2C–Br–Cl$	S_1	628 (0.0002)	532 (0.0002)	–
	S_2	567 (0.0003)	488 (0.0116)	–
	S_3	448 (0.1895)	440 (0.2216)	–
	S_4	349 (0.0001)	328 (0.0002)	–
	S_5	325 (0.0824)	303 (0.1354)	–
	S_6	303 (0.0000)	279 (0.0041)	–
	S_7	294 (0.0065)	263 (0.0559)	–
	S_8	283 (0.0022)	257 (0.0270)	–
	S_9	273 (0.2196)	252 (0.0330)	–
	S_{10}	272 (0.0509)	236 (0.1136)	–
ClBrC–Br–Br	S_1	700 (0.0001)	606 (0.0002)	–
	S_2	644 (0.0004)	561 (0.0004)	–
	S_3	464 (0.2420)	451 (0.2939)	–
	S_4	332 (0.0480)	315 (0.0004)	–
	S_5	329 (0.0549)	305 (0.1492)	–
	S_6	301 (0.0005)	265 (0.0023)	–
	S_7	279 (0.0508)	258 (0.0017)	–
	S_8	278 (0.1214)	251 (0.0571)	–
	S_9	265 (0.0556)	241 (0.1179)	–
	S_{10}	249 (0.0473)	235 (0.0804)	–
$Br_2C–Cl–Br$	S_1	778 (0.0000)	674 (0.0001)	–
	S_2	736 (0.0002)	640 (0.0002)	–
	S_3	436 (0.3520)	421 (0.4277)	–
	S_4	358 (0.0691)	324 (0.0608)	–
	S_5	331 (0.0000)	308 (0.0001)	–
	S_6	313 (0.0001)	261 (0.0017)	–
	S_7	301 (0.0729)	256 (0.0412)	–
	S_8	275 (0.0492)	252 (0.0165)	–
	S_9	271 (0.0177)	250 (0.0608)	–
	S_{10}	253 (0.0084)	242 (0.0219)	–
$Br_2C–Br–Br$	S_1	699 (0.0001)	608 (0.0002)	–
	S_2	644 (0.0003)	562 (0.0004)	645 (0.02)
	S_3	471 (0.2316)	457 (0.2843)	458 (0.43)
	S_4	349 (0.1110)	329 (0.0003)	337 (0.12)
	S_5	348 (0.0001)	324 (0.1519)	–
	S_6	314 (0.0000)	278 (0.0059)	–
	S_7	292 (0.0109)	268 (0.0011)	–
	S_8	291 (0.1060)	264 (0.0342)	–
	S_9	281 (0.1095)	254 (0.0531)	–
	S_{10}	273 (0.0407)	250 (0.1547)	–

Extending these studies to the other substituted tribromomethanes, Fig. 3 shows a matrix infrared spectrum of a $CClBr_3$:Ar (~1:500) sample at ~5 K following laser photolysis at 220 nm. Note that the 220 nm photon energy (544 kJ/mol) is far in excess of thermochemical thresholds for both C–Cl (293 kJ/mol) and C–Br

(232 kJ/mol) bond homolysis,[35] and therefore three different iso-species can be formed (Fig. 2). First, C–Br bond cleavage and subsequent Br–Br bond formation leading to ClBrC–Br–Br; second, C–Br bond cleavage and Cl–Br bond formation leading to Br_2C–Cl–Br; and third, C–Cl bond cleavage followed by Cl–Br bond formation leading to Br_2C–Br–Cl. Calculations at the B3LYP/aug-cc-pVTZ level (ZPE corrected) predict that ClBrC–Br–Br is the most stable of the three, lying 16.4 kJ/mol below Br_2C–Cl–Br, and 24.8 kJ/mol below Br_2C–Br–Cl. The predicted (B3LYP/aug-cc-pVTZ) IR spectra of these three isomers in the C–Cl and C–Br stretching region is shown in Fig. 3, and the calculated frequencies are given in Table 3. Two isomers, ClBrC–Br–Br and Br_2C–Br–Cl, are clearly observed, with diagnostic bands at, respectively, 879 and 779 cm^{-1}. These isomers result from cleavage of the C–Br and C–Cl bonds, respectively, in the parent. Using the calculated (B3LYP/aug-cc-pVTZ) intensities, we derive a ratio of 1.4 for the column density of ClBrC–Br–Br to Br_2C–Br–Cl following photolysis of the parent. The third isomer, Br_2C–Cl–Br is formed in very small yield, if at all (Fig. 3). If the sample was characterized by a Boltzmann distribution at 5 K, a ratio of ClBrC–Br–Br to Br_2C–Br–Cl of 27 is predicted based upon the relative energies calculated above.

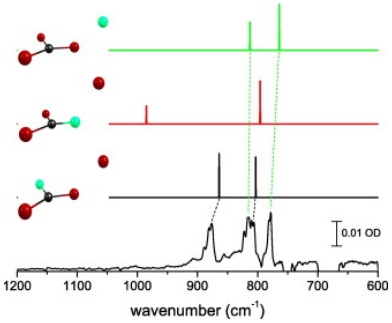

Fig. 3. Observed difference IR spectrum following 220 nm laser photolysis of a $CClBr_3$:Ar sample held at 5 K and calculated (B3LYP/aug-cc-pVTZ) infrared spectra of the three possible iso-$CClBr_3$ isomers. The calculated spectra are shown as stick spectra and the intensities are arbitrarily scaled; quantitative information is provided in Table 3.

Table 3. Observed and calculated vibrational frequencies (in cm^{-1}) of the various isomers of iso-$CClBr_3$. Calculations were performed with the methods shown and an aug-cc-pVTZ basis. Calculated intensities in km/mol are given in parentheses.

Species	Mode	Approx. Descr.	Calc. (B3LYP)	Calc. (M06)	Calc. (MP2)	Obs. (this work; Ar)
Br_2C–Br–Cl	ν_1	C–Br stretch	813 (114)	872 (99)	944 (38)	816
	ν_2	Asym. C–Br stretch	763 (186)	787 (153)	815 (128)	779
	ν_3	C–Br_3 rock	366 (7)	349 (7)	350 (37)	–
	ν_4	Sym. C–Br stretch	282 (34)	299 (32)	324 (4)	–
	ν_5	Cl–Br stretch	223 (84)	217 (110)	281 (5)	–
	ν_6	C–Br wag	186 (0)	184 (0)	188 (0)	–
	ν_7	Br–C–Br bend	163 (0)	163 (1)	169 (0)	–
	ν_8	Torsion	64 (2)	62 (2)	60 (2)	–
	ν_9	C–Br–Cl bend	42 (9)	45 (9)	59 (2)	–
ClBrC–Br–Br	ν_1	C–Cl stretch	864 (179)	900 (182)	965 (56)	878
	ν_2	Asym. C–Br stretch	803 (165)	833 (151)	865 (133)	809
	ν_3	C–Cl wag	367 (11)	362 (19)	401 (28)	–
	ν_4	Sym. C–Br stretch	347 (39)	350 (28)	332 (10)	–
	ν_5	Cl–C–Br bend	220 (3)	221 (4)	236 (1)	–
	ν_6	Br–C–Br bend	195 (15)	194 (15)	219 (0.1)	–
	ν_7	Br–Br stretch	155 (30)	157 (40)	193 (0.4)	–
	ν_8	Torsion	59 (1)	58 (1)	59 (1)	–
	ν_9	C–Br–Br bend	38 (4)	39 (5)	46 (1)	–

$Br_2C–Cl–Br$	ν_1	C–Cl stretch	984 (74)	1014 (65)	982 (41)	–
	ν_2	Asym. C–Br stretch	796 (175)	830 (153)	829 (141)	–
	ν_3	C–Br stretch	373 (25)	379 (41)	417 (20)	–
	ν_4	C–Br_3 rock	348 (53)	339 (36)	353 (7)	–
	ν_5	C–Cl wag	245 (0)	246 (0)	279 (14)	–
	ν_6	Cl–Br stretch	197 (28)	193 (34)	246 (0.1)	–
	ν_7	Br–C–Cl bend	171 (12)	168 (18)	182 (0.3)	–
	ν_8	C–Cl–Br bend	52 (4)	46 (1)	55 (1)	–
	ν_9	Torsion	49 (1)	41 (4)	49 (0)	–

The UV–Vis spectra are also consistent with the formation of more than one iso-$CClBr_3$ isomer. Fig. 4compares the observed spectrum of a $CClBr_3$:Ar (~1:500) sample at ~5 K following laser photolysis at 220 nm with TDDFT predictions of the electronic absorptions of the three iso-species. All three isomers are predicted to have strong absorptions in the 400–450 nm region (Table 2), consistent with the broad and intense feature observed experimentally. In addition, the $Br_2C–Br–Cl$ isomer is predicted to have a nearly equally strong absorption in the UV, which lies near the position of a strong band observed at 254 nm (Fig. 4).

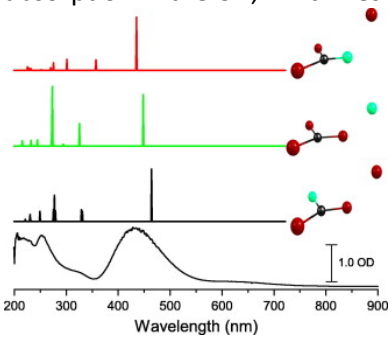

Fig. 4. UV–Vis spectrum following 220 nm laser photolysis of a $CClBr_3$:Ar sample held at 5 K and calculated (TD M06/aug-cc-pVTZ) electronic spectra of the three possible iso-$CClBr_3$ isomers. The calculated spectra are shown as stick spectra and the intensities are arbitrarily scaled; quantitative information is provided in Table 2.

As discussed in the introduction, in comparison with $CFBr_3$ and $CClBr_3$ the photodissociation of CBr_4in condensed phases has been more extensively studied, albeit with sometimes conflicting results. Fig. 2 shows the calculated geometrical parameters of this isomer, while in Fig. 5 we show infrared spectra of: (a) a CBr_4:Ar (~1:500) sample at ~5 K, (b) a difference spectrum following 266 nm photolysis, and (c) a difference spectrum following photolysis, annealing to 30 K, and recooling to 5 K. In panel (b), the calculated IR spectrum of iso-CBr_4 at the M06/aug-cc-pVTZ level is shown. It is apparent that after photolysis both the isomer and the carbene CBr_2 are formed; the latter is assigned to the strong feature at 632 cm^{-1} in panel (b). The CBr_3 radical may also be formed, but conclusive evidence is lacking, as the strongest IR absorption of this radical (at 778 cm^{-1}) overlaps the strongest absorption of the iso-species. Upon annealing, the 632 cm^{-1} absorption disappears, while the isomer absorptions increase, as shown in panel (c). The observed IR absorptions of the isomer (Table 4) are in good agreement with theory. Fig. 6 shows the UV–Vis spectrum of the isomer, which is compared with the predicted spectrum at the TD M06/aug-cc-pVTZ level. Using Eq. (1), the derived oscillator strength of the most prominent band of iso-CBr_4 at 458 nm is 0.43 (ε_{max} ~ 23,000 L mol^{-1} cm^{-1}), in reasonable agreement with the TDDFT predictions (Table 2).

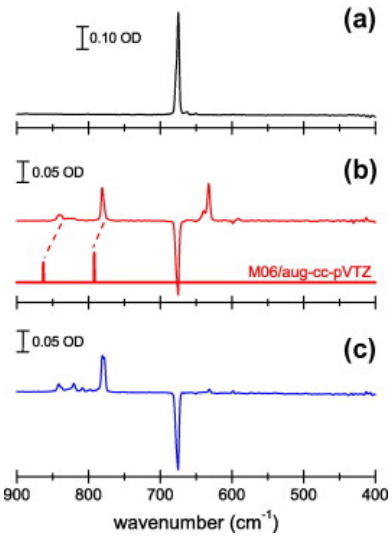

Fig. 5. (a) Infrared (IR) spectrum of a CBr_4:Ar sample at 5 K. (b) Difference IR spectrum following photolysis of the sample at 266 nm. The calculated (M06/aug-cc-pVTZ) spectrum of iso-CBr_4 is shown as a stick spectrum in this panel, and the intensity is arbitrarily scaled; quantitative information is provided in Table 4. (c) Difference IR spectrum following photolysis at 266 nm and subsequent annealing to 30 K, following be recooling to 5 K.

Table 4. Observed and calculated vibrational frequencies (in cm^{-1}) of iso-CBr_4. Calculations were performed with the methods shown and an aug-cc-pVTZ basis. Calculated intensities in km/mol are given in parentheses.

Mode	Approx. Descr.	Calc. (B3LYP)	Calc. (M06)	Calc. (MP2)	Obs. (this work; Ar)	Obs. [26]
ν_1	C–Br stretch	815 (115)	863 (97)	928 (43)	842	828
ν_2	Asym. C–Br stretch	760 (174)	793 (144)	814 (123)	781	–
ν_3	C–Br_3 rock	342 (20)	328 (21)	355 (28)	–	–
ν_4	Sym. C–Br stretch	282 (29)	296 (24)	294 (3)	–	–
ν_5	C–Br rock	181 (0)	180 (0)	225 (0)	–	–
ν_6	C–Br_2 rock	174 (26)	171 (33)	184 (0)	–	179
ν_7	Br–Br stretch	148 (18)	149 (22)	167 (2)	–	155
ν_8	Torsion	50 (1)	50 (1)	46 (0)	–	–
ν_9	C–Br–Br bend	35 (4)	37 (4)	46 (1)	–	–

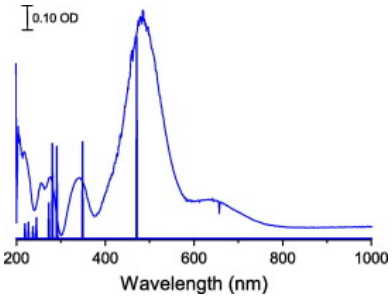

Fig. 6. UV–Vis spectrum of a CBr_4:Ar sample at 5 K following photolysis at 266 nm. The calculated (TDM06/aug-cc-pVTZ) spectrum of iso-CBr_4 is shown as a stick spectrum with arbitrarily scaled intensity; for quantitative information see Table 2.

3.2. Structure and bonding in iso-$CXBr_3$ and the $CXBr_3$ Potential Energy Surface

Theory confirms that the iso-$CXBr_3$ (X = F, Cl, Br) species are local minima on the respective $CXBr_3$Potential Energy Surfaces (PESs). We characterized selected stationary points on these PESs using single point CCSD(T)/aug-cc-pVTZ calculations on the MP2 optimized structures. The CCSD(T) energies, shown for $CFBr_3$ in Fig. 7, indicate that iso-$CFBr_3$ is bound relative to the radical ($CFBr_2$ + Br) asymptote by 53 kJ/mol. In

contrast, the stationary point corresponding to molecular products ($CFBr + Br_2$) lies 48 kJ/mol [CCSD(T)//MP2] above the iso-$CFBr_3$ minimum. The $CFBr_3$ PES resembles other halon PESs we have examined, including CF_2Br_2 [22], CF_2Cl_2 [22], and $CHBr_3$ [21], where the isomerization transition state (TS) lies energetically near (and sometimes below) the threshold for radical products. Thus, in reactions taking place on the ground potential surface, isomerization will compete with simple bond fission. The isomer, once formed, can decay via Br–Br or C–Br bond fission to yield radical ($CFBr_2 + Br$) or molecular ($CFBr + Br_2$) products, respectively. Relaxed scans along the Br–Br and C–Br coordinates of the isomer show that there is no barrier to dissociation for either the radical or molecular channels.

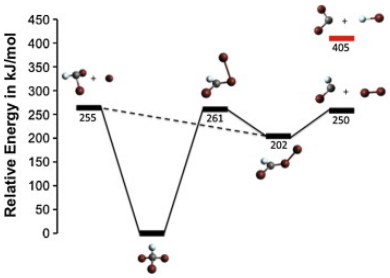

Fig. 7. Calculated (CCSDT//MP2/aug-cc-pVTZ) stationary points on the $CFBr_3$ potential energy surface. All energies are given in kJ/mol.

The situation is similar for $CClBr_3$ and CBr_4. At the same level of theory, the lowest energy iso-$CClBr_3$minimum (i.e., ClBr–C–Br–Br) is bound relative to the radical ($CClBr_2 + Br$) asymptote by 66 kJ/mol, while the molecular ($CClBr + Br_2$) asymptote lies 87 kJ/mol above this minimum. These numbers are similar for iso-CBr_4, which is bound relative to the radical ($CBr_3 + Br$) asymptote by 63 kJ/mol, and the molecular ($CBr_2 + Br_2$) asymptote lies 96 kJ/mol above the iso-CBr_4 minimum. In this case, the calculated isomerization barrier lies 15 kJ/mol below the threshold to radical products. Graphs of the calculated stationary points on the PESs of $CClBr_3$ and CBr_4 are shown in Figures S1 and S2 in the supporting information.

To further examine bonding in this series, each of the iso-halon species of the iso-$CXBr_2$–Br (X = F, Cl, Br) series was examined with MP2/aug-cc-pVTZ calculations using NBO 5.9 implemented in Gaussian 09.[33] First, intrinsic reaction coordinate calculations were performed to characterize the isomerization path. Next, the bonding of each iso-halon species, as well as each IRC point between the halon and iso species, were analyzed using Natural Resonance Theory,[36], [37], [38] and the details of these calculations are provided in the supporting information. Fig. 8 shows an illustrative plot of the resonance structure weights along the reaction coordinate in the isomerization of $CFBr_3$; corresponding plots for $CClBr_3$ and CBr_4 are shown in Figures S3 and S4 in the supporting information. The most important resonance structures (weights >5%) correspond to covalent, ion-pair, and ylide structures, identified in the figures. As with the isomerization of other halons,[21], [39] these species convert from a primarily covalent structure to an iso-form that is dominated by an ion pair resonance form. This can be easily noted in the increased bond order between C and Br (4) in each of the cases, showing the contribution of a partial double bond between those two atoms (Table S1; supporting information). Additionally, like other iso-halon species, the central carbon maintains a weak bond to the external bromine atom [Br (5)] in each of these three cases of 0.22, 0.19, and 0.27 for X = F, Cl, Br respectively (Tables S2–S4; supporting information). The fluorine substituted case results in the greatest bond order between Br (4) and Br (5), presumably due to the greater polarization of the iso-halon due to the presence of the fluorine atom. The atomic charges support this interpretation, as the fluorine atom is the only negatively charged atom of the X = F, Cl, Br series, which results in an increase in the ionic contribution to the bond order for Br (4)–Br (5) from 0.0637 for CBr_4 to 0.1567 for $CFBr_3$.

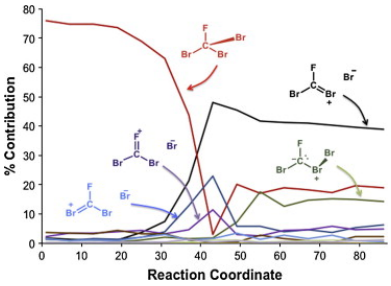

Fig. 8. Calculated resonance structure weights along the IRC path in the isomerization of $CFBr_3$, using Natural Resonance Theory analysis at the MP2/aug-cc-pVTZ level. The transition state, located near point 40, represents a cross-over from covalent to ion-pair binding. The five resonance structures with the largest weights are identified.

Possibly the most surprising observation is the relative lack of change of halon substitution on the overall NBO/NRT analysis of these molecules. In each of the cases, the relative contributions of each of the resonance structures is fairly consistent at 37%, 39% and 39% for X = F, Cl, Br respectively (Table S1; supporting information). There is a slight reduction in the contribution of the three main resonance structures for the fluorine substituted species compared to the chlorine- and bromine-substituted ones.

In view of the NBO/NRT analysis, it is not surprising that the formation and decay rates of the isomer will be very sensitive to environment, as there is a differential solvation of the iso-form and isomerization transition state relative to the parent isomer. Consider the CBr_4 potential energy surface, where the calculations of Ihee and co-workers show that the isomerization barrier from CBr_4 to iso-CBr_4 is lowered by some 32 kJ/mol in methanol as compared with the gas-phase, and the iso-CBr_4 well is lowered by a similar amount.[30] In contrast, the radical and molecular thresholds are nearly the same in the two environments. Thus, in condensed phases the isomer is stabilized with respect to C–Br or Br–Br bond cleavage, so that back isomerization to the parent halon is the lowest energy channel.

3.3. Photoisomerization of iso-$CXBr_3$

Following stabilization of the iso-species in the matrix, we conducted studies of the photochemistry of the isomer by irradiating into the strongest transition, in each case the $S_0 \rightarrow S_3$ transition (Table 2). As illustrated in Fig. 9 for iso-$CFBr_3$, photoexcitation leads to loss of the iso-form and regeneration of the parent halon. This "photoisomerization" process was noted in the first studies of the iso-halons by Maier and co-workers.[23], [24], [25] Although our IRC calculations show that the two isomers are connected by a first-order saddle point, the exact mechanism of the photoisomerization process has not been firmly established. In future experiments, we plan to use Resonance Raman spectroscopy to probe the short time dynamics following photoexcitation.

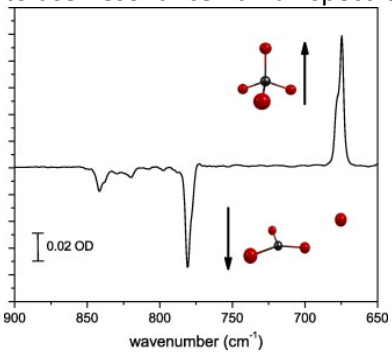

Fig. 9. Difference spectrum following 440 nm excitation of matrix-isolated iso-CBr_4. Laser irradiation of the isomer leads to loss of the isomer IR bands and reformation of the parent halon.

4. Conclusions

We have examined the structure, spectroscopy, photochemistry, and isomerization pathways of substituted iso-tribromomethanes (iso-$CXBr_3$; X = F, Cl, Br). These species were trapped in rare gas matrices, and

their IR and UV–Vis spectra recorded, which were compared with the predictions of *ab initio* and Density Functional Theory (DFT) calculations using high quality basis sets. Generally, excellent agreement is found amongst the different levels of theory. Various stationary points on the $CXBr_3$ Potential Energy Surfaces (PESs) were characterized computationally using DFT, MP2, and CCSD (T) methods. Calculations reveal that the isomers exist in relatively deep wells on the respective PESs. For example, CCSD (T)//MP2/aug-cc-pVTZ calculations indicate that iso-$CFBr_3$ is bound relative to the radical ($CFBr_2$ + Br) asymptote by 53 kJ/mol, whereas the stationary point corresponding to molecular products (CFBr + Br_2) lies 48 kJ/mol above the iso-$CFBr_3$ minimum. On the $CClBr_3$ and CBr_4 PESs, the isomer well is deeper. Our intrinsic reaction coordinate (IRC) calculations reveal that a first-order saddle point connects the two isomers, and the barrier to isomerization in the gas-phase is energetically near the threshold for simple bond fission. In condensed phases, the ion pair dominated iso-structure (revealed by NRT calculations) is further stabilized with respect to these thresholds, indicating that back isomerization will be the most favorable decay pathway.

Laser irradiation of the isomers resulted in reformation of the parent $CXBr_3$, although the exact mechanism (i.e., photoisomerization vs. dissociation followed by geminate recombination) has not yet been established. This forms the basis for future work on this important set of reactive intermediates.

Acknowledgements

Support of the National Science Foundation [CHE-0717960 (S.A.R.); CHE-1011959 (R.J.M.)] and the donors of the Petroleum Research Fund of the American Chemical Society [48740-ND6 (S.A.R.)]. This research was supported in part by National Science Foundation Grant CHE-0840494 (UW Phoenix computer cluster). The authors thank Khushabu Thakur and Professor Rajendra Rathore for assistance in synthesizing the $CClBr_3$ sample.

Appendix A. Supplementary data

Download Word document (313KB)Help with doc files

Supporting information. Supplementary material contains Figs. S1–S4 and Tables. S1–S4.

References

[1] L.T. Molina, M.J. Molina. *J. Phys. Chem*., 87 (1983), pp. 1306-1308
[2] L.A. Barrie, J.W. Bottenheim, R.C. Schnell, P.J. Crutzen, R.A. Rasmussen. *Nature*, 334 (1988), pp. 138-141
[3] K. Ranajit, G. Talukdar, L. Vaghjiani, A.R. Ravishankara. *J. Chem. Phys*., 96 (1992), pp. 8194-8201
[4] J.E. Thompson, A.R. Ravishankara. *Int. J. Chem. Kin*., 25 (1993), pp. 479-487
[5] V.L. Orkin, E.E. Kasimovskaya. *J. Atmos. Chem*., 21 (1995), pp. 1-11
[6] G.F. Cota, W.T. Sturges. *Mar. Chem*., 56 (1997), pp. 181-192
[7] S.M. Schauffler, E.L. Atlas, F. Flocke, R.A. Lueb, V. Stroud, W. Travnicek. *Geophys. Res. Lett*., 25 (1998), pp. 317-320
[8] V.L. Dvortsov, M.A. Geller, S. Solomon, S.M. Schauffler, E.L. Atlas, D.R. Blake. *Geophys. Res. Lett*., 26 (1999), pp. 1699-1702
[9] W.S. McGivern, O. Sorkhabi, A.G. Suits, A. Derecskei-Kovacs, S.W. North. *J. Phys. Chem. A*, 104 (2000), pp. 10085-10091
[10] K.A. Peterson, J.S. Francisco. *J. Chem. Phys*., 117 (2002), pp. 6103-6107
[11] D.D. Xu, J.S. Francisco, J. Huang, W.M. Jackson. *J. Chem. Phys*., 117 (2002), pp. 2578-2585
[12] K.D. Bayes, D.W. Toohey, R.R. Friedl, S.P. Sander. *J. Geophys. Res. Atmos*., 108 (2003), pp. 4095-4101
[13] H.Y. Huang, W.T. Chuang, R.C. Sharma, C.Y. Hsu, K.C. Lin, C.H. Hu. *J. Chem. Phys*., 121 (2004), pp. 5253-5260
[14] W.M. Kwok, C. Zhao, Y.-L. Li, X. Guan, D.L. Phillips. *J. Chem. Phys*., 120 (2004), pp. 3323-3332
[15] W.M. Kwok, C. Zhao, Y.-L. Li, X. Guan, D. Wang, D.L. Phillips. *J. Am. Chem. Soc*., 126 (2004), pp. 3119-3131
[16] B.J. Petro, E.D. Tweeten, R.W. Quandt. *J. Phys. Chem. A*, 108 (2004), pp. 384-391
[17] Y. Tang, L. Ji, B.F. Tang, R.S. Zhu, S. Zhang, B. Zhang. *Chem. Phys. Lett*., 392 (2004), pp. 493-497
[18] S.L. Carrier, T.J. Preston, M. Dutta, A.C. Crowther, F.F. Crim. *J. Phys. Chem. A*, 114 (2010), pp. 1548-1555

[19] J.P. Simons, P.E.R. Tatham. *J. Chem. Soc. A* (1966), pp. 854-859
[20] G.P. Brown, J.P. Simons. *Trans. Faraday Soc*., 65 (1969), p. 3245
[21] L. George, A. Kalume, J. Wagner, B.J. Esselman, R.J. McMahon, S.A. Reid. *J. Chem. Phys*., 135 (2011), p. 124503
[22] A. Kalume, L. George, S.A. Reid. *J. Phys. Chem. Lett*., 1 (2010), pp. 3090-3095
[23] G. Maier, H.P. Reisenauer. *Angew. Chem.-Int. Ed. Eng*., 25 (1986), pp. 819-822
[24] G. Maier, H.P. Reisenauer, J. Hu, B.A. Hess, L.J. Schaad. *Tetrahedron Lett*., 30 (1989), pp. 4105-4108
[25] G. Maier, H.P. Reisenauer, J. Hu, L.J. Schaad, B.A. Hess. *J. Am. Chem. Soc*., 112 (1990), pp. 5117-5122
[26] X. Zheng, W.H. Fang, D.L. Phillips. *J. Chem. Phys*., 113 (2000), p. 10934
[27] C. Zhao, X. Lin, W.M. Kwok, X. Guan, Y. Du, D. Wang, K.F. Hung, D.L. Phillips. *Chem. Eur. J*., 11 (2005), pp. 1093-1108
[28] H. Zhang, A.S. Dvornikov, P.M. Rentzepis. *J. Phys. Chem. A*, 109 (2005), pp. 5984-5988
[29] Q. Kong, M. Wulff, J.H. Lee, S. Bratos, H. Ihee. *J. Am. Chem. Soc*., 129 (2007), pp. 13584-13591
[30] Q. Kong, M. Wulff, S. Bratos, R. Vuilleumier, H. Ihee. *J. Phys. Chem. A*, 110 (2006), pp. 11178-11187
[31] L. George, A. Kalume, P.Z. El-Khoury, A. Tarnovsky, S.A. Reid. *J. Chem. Phys*., 132 (2010), p. 084503
[32] P.A. Morken, P.C. Bachand, D.C. Swenson, D.J. Burton. *J. Am. Chem. Soc*., 115 (1993), p. 5430
[33] M.J. Frisch, et al., *GAUSSIAN* 09, Rev. A.1, 2009.
[34] E.D. Glendening, J.K. Badenhoop, A.E. Reed, J.E. Carpenter, J.A. Bohmann, C.M. Morales, F. Weinhold, NBO Version 3.1, 2011.
[35] A.A. Zavitsas. *J. Phys. Chem*., 91 (1987), pp. 5573-5577
[36] E.D. Glendening, F. Weinhold. *J. Comput. Chem*., 19 (1998), pp. 593-609
[37] E.D. Glendening, F. Weinhold. *J. Comput. Chem*., 19 (1998), pp. 610-627
[38] E.D. Glendening, J.K. Badenhoop, F. Weinhold. *J. Comput. Chem*., 19 (1998), pp. 628-646
[39] T.J. Preston, M. Dutta, B.J. Esselman, A. Kalume, L. George, R.J. McMahon, S.A. Reid, F.F. Crim. *J. Chem. Phys*., 135 (2011), p. 114503